LETTER

3D Ordered Assemblies of Semiconductive Micro/Nanowires Using Microscale Fibrous Building Blocks

Yan Hong, Zeyu Ma, Chaoming Wang, Liyuan Ma, and Ming Su*

NanoScience Technology Center, Department of Mechanical, Materials and Aerospace Engineering, University of Central Florida, Orlando, Florida 32826

ABSTRACT Three-dimensional (3D) ordered assemblies of semiconductive micro/nanowires are made by match-stick assembly of fibrous building blocks (FBBs). A glass tube filled with powders of starting material is processed drawn into centimeter-long, micrometer-diameter FBBs with controlled diameter and spacing. By repeating a draw-cut-stack process, the diameter and spacing of filling material can be programmably reduced from millimeters to hundreds of nanometers. The FBBs are densely packed into 3D ordered structures such that wires in one layer are at defined angle (θ) relative to those in the adjacent layers, where θ is between 0 and 180°. The electrical measurements at bundled wires and single wire level confirm semiconducting behavior of wires. By directly manipulating microscale FBBs, the method allows high yield production of 3D ordered micro/nanowires with controlled position and orientation, enabling the construction of a new class of micro/nanomaterials.

KEYWORDS: 3D ordered assembly • fibrous building blocks • semiconductive micro/nanowires • fiber-drawing nanomanufacturing • programmed size reduction

Micro/nanowires have attracted extensive attention because of their potential uses as components for future electronics, mechanics, spintronics, optics, sensing devices, etc. (1−3). Such one-dimensional materials with small diameters are prepared by either bottom-up synthesis or top-down size reduction. In the first case, molecular or atomic precursors are assembled or deposited by physical or chemical vapor deposition, hydrothermal synthesis, and template-based deposition (4−9). The diameters of thus-obtained wires are determined by diameters of catalyst nanoparticles or porous templates (10, 11). In the second case, a bulk starting material is mechanically deformed (drawing, spinning, and extruding) to one-dimensional structures (12−14). Such top-down methods include electrospinning of polymer nanofibers, drawing metallic fibers, and extruding wires through small diameter dies. In contrast to bottom-up methods, the diameter control in the top-down method is achieved by adjusting operating parameters, such as voltage and viscosity (electrospinning), drawing temperature, and speed (fiber-drawing), die diameter and pressure (extruding).

To achieve desired functions, the positions, spacings, and orientations of micro/nanowires should be controlled with high precision. Such wires can be aligned in two-dimensional plane by using electrical field, hydrodynamic flow, expanding balloons, or direct manipulating (15−19). In addition, template- or surface-directed deposition and vapor deposition can also make aligned nanowires (20, 21). However, there is no controlled method currently available that can make ordered 3D micro/nanowire structures at high yield. Electrospinning makes randomly tangled nanowires, and extruding makes individual wires rather than an ordered network. Such a deficiency in fabrication ability has consequently led to the lack of fundamental knowledge on the effect of 3D ordered structure. On the other hand, a variety of methods (vapor deposition or dielectrophoresis) occasionally make random 3D networks of micro/nanowires (22−27); however, these methods do not have sufficient controls over the length and diameter of single wires and the ordering (position, spacing, and orientation) of wires in 3D networks, and thus cannot support a systematic study on the effects of structural ordering.

Fiber-drawing nanomanufacturing (FDN) can be used to make a variety of micro/nanostructures, such as copper alloy sheathed iron wires, glass nanochannel and nanocone arrays, and glass-encapsulated metallic micro/nanowires (28−31). This method offers precise controls over the diameter, length, and interwire spacing of micro/nanowires and has high production yield. However, to make 3D ordered micro/nanowire arrays, a conceptually new strategy should be developed. Rather than simply targeting productions of micro/nanowires, in this work, we will describe the method to construct 3D assembly of semiconductive nanowires by using microscale fibrous building blocks (FBBs) obtained through FDN process using lead telluride (PbTe) as example. The process of fabricating FBBs of semiconductor wires can be described as following. Pouring PbTe raw powders into a glass tube makes a preform for fiber drawing. The fibers obtained from the first draw cycle are cut into short pieces of equal length that are stacked together to form

* Corresponding author. E-mail: mingsu@mail.ucf.edu.
Received for review November 7, 2008 and accepted January 16, 2009

DOI: 10.1021/am800171t

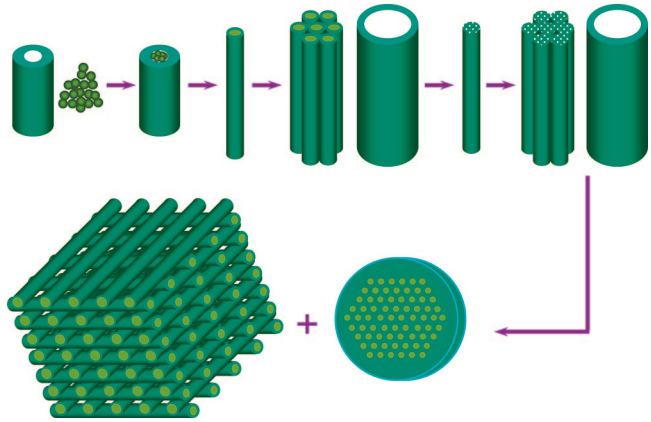

FIGURE 1. 3D assemblies of semiconductive nanowires produced from fibrous building blocks.

a hexagonal fiber bundle for the next draw cycle. By repeating the same draw-cut-stack process for several times, both the thickness of the glass tube and the diameter of PbTe wire decrease from centimeter to hundreds nanometer. After the last draw, the short fibers are assembled in a layer-by-layer manner, where the wire orientations in one layer are at certain angle (θ) to those of adjacent layers, forming an orthogonal array of aligned fibers (Figure 1). The θ can be changed from 0 to 180°. In case of 0°, the nanowires are aligned in parallel. Such a method allows the manipulation of ten thousand wires at the same time. In addition, during fiber drawing and annealing process, the glass tube is connected to a vacuum pump, which allows an intimate contact between the glass tube and PbTe material and helps to minimize the oxidation of micro/nanowires.

PbTe powders with an average grain size of 8 μm are obtained from Aldrich and filled into an acid-resistant Pyrex glass tube. Usually, 15 g of the powders are packed at a density of 7.5 g/mL inside a glass tube with an internal volume of 2 mL. Because the density of PbTe solid is 8.2 g/cm^3, 8% of the glass tube will be occupied by air that is trapped between the PbTe powders. The softening temperature of the glass is 825 °C and the melting temperature of PbTe is 905 °C. The fiber drawing is carried out at 960 °C. The glass feed and the drawing speeds are determined by the glass tube and fibers to be 0.008 and 1.8 m/s, respectively. Figure 2A shows a scanning electron microscopy (SEM) image of an array of hexagonally ordered microwires. Such an array is generated by annealing a bundle of first drawn fibers at 800 °C to make a rod, cutting the rod perpendicular its axis to make plates and polishing the plates using grits of different grade. Figure 2B shows a broken glass fiber that contains a 100 μm diameter wire obtained from the first draw cycle. The bundled glass-wire composite rod is drawn again to reduce the diameter. Figure 2C shows the cross-section image of the wire, where the diameters of microwires are reduced to 5 μm. The glass shells around each PbTe wire can be removed by immersing fibers into a 2% hydrogen fluoride aqueous solution for 10 h. Figure 2D shows the SEM image of long wires after the second draw cycle, where the diameter of the wire is about 5 μm. Images E and F in Figure 2 are images of PbTe microwires after the third draw cycle. The glass shells have been removed to indicate the diameter of microwires (1−2 μm). A glass microtube can be seen clearly in the left part of Figure 2F, confirming the formation of PbTe microwires. As the diameter becomes smaller, the wires are short, probably because of the fragility of small diameter wires. In the last, the annealed bundle of the third-drawn wires is further stretched at 850 °C to four times as long as its original length. Figure 2G is the cross-section SEM image of one stretched nanowire. The flat top of the nanowire is induced by the polishing process. After the glass shell is removed, the diameter of the PbTe nanowire is about 400 nm, as shown in Figure 2H, where a few broken glass nanotubes can also be found in the left part of the image.

Not only are they bundled together to form micro/nanowires aligned in parallel but the short glass fibers containing PbTe have been assembled into a layer-by-layer fashion, where the fibers in odd numbers of layers will be oriented that certain angle relative to those fibers in even numbers of layers. In principle, nanowires in one layer can be assembled at a nonzero angle relative to those in the adjacent layers. We have made a cubic stainless-steel container (5 × 5 × 5 cm^3) that can be dissembled and reassembled. The top cover of the container is a movable plate that allows a constant pressure to be applied. The FBBs from each draw cycle are cut into short and equal length and packed densely into the container. The assembly is annealed at 800 °C in air for 2 h. After being cooled to room temperature, the container is dissembled from sides, leaving a glass-semiconductor wire composite cube. Subsequently, each side of the composite cube is polished using grits of different grade. To expose the semiconductor wires inside the composite cubes, we have used polyacrylic to block certain area on each side of the cube, and etched glass by dipping the cube into a 4% hydrogen fluoride solution. Images A and B in Figure 3 are the SEM images of the assembled wires obtained in the first draw cycle. Images C and D in Figure 3 are the SEM images of a 3D network of PbTe microwires from the second draw cycle. In these four images, the wires perpendicular to the observation direction can be seen as circles. The FBBs containing nanowires are assembled into similar perpendicular configuration using the same rectangular mold, but the SEM images (not shown) cannot resolve individual nanowires and the microscale configuration at the same time and are very similar to that of Figure 2G. Furthermore, we have removed the glass shells around PbTe wires from the first draw by immersing the 3D structure into the hydrogen fluoride for 24 h (images E and F in Figure 3), where the PbTe wires and residual glass shell can be seen clearly. The SEM images show a higher brightness of the core than the residual shell, which further confirms the high electron conductivity of the PbTe wires.

The compositions of PbTe wires after each draw-cut-stack cycle have been studied by energy dispersive X-ray analysis (EDX). Figure 4A shows strong peaks of lead and tellurium, where the four curves are collected from the raw powder, the first, second, and third drawn wires (from bottom to top).

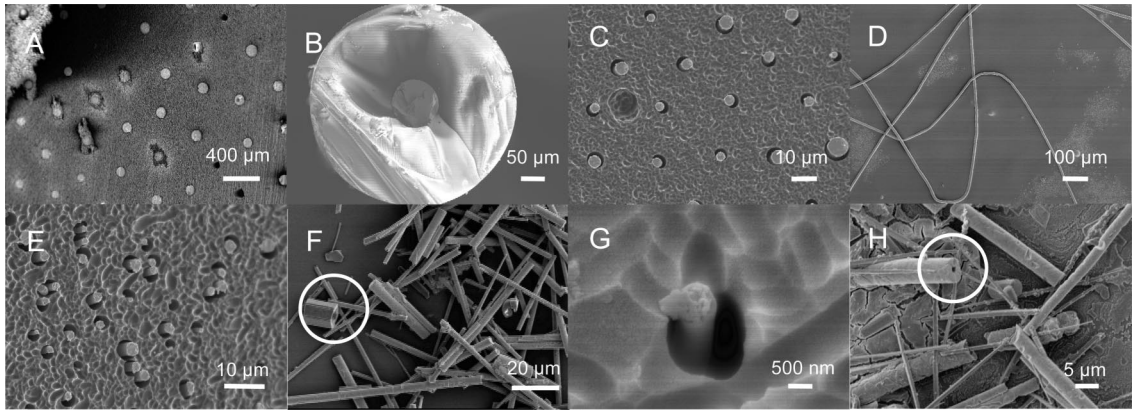

FIGURE 2. SEM images of (A) a microwire array and a (B) glass encapsulated microwire after the first draw. SEM images of a (C) microwire array and (D) single microwire after the second draw. SEM images of (E) a microwire array (F) and microwires after the third draw. SEM images of (G) an embedded nanowire and (H) nanowires without glass shell after stretching. The glass shells around PbTe wires in the images of D, F, and H are removed before imaging. Some broken glass tubes can also be seen in F and G.

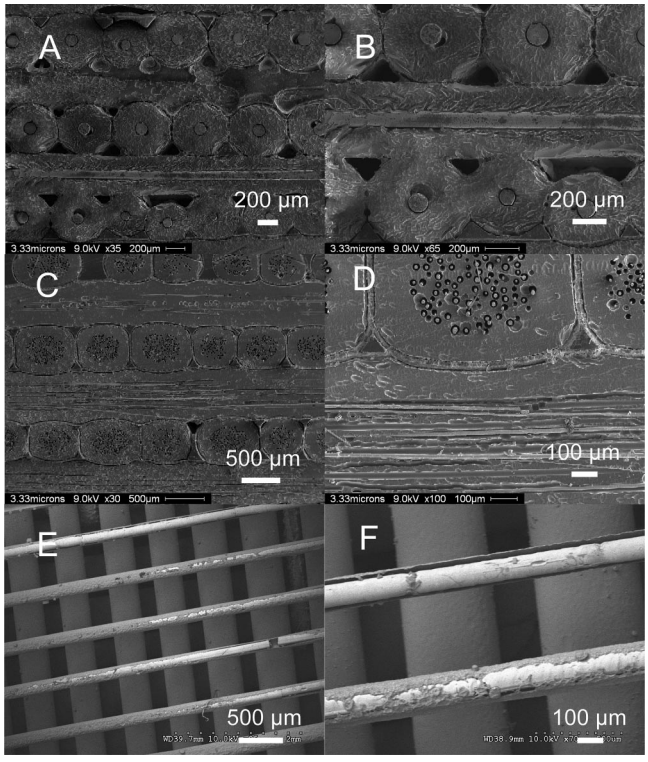

FIGURE 3. SEM images of (A, B) the orthogonally assembled microwires obtained from the first draw cycle and (C, D) microwires obtained from the second draw cycle. (E, F) SEM images of 3D aligned PbTe wires from first draw after removing glass shells by chemical etching.

The relative amounts of lead and tellurium are determined by calibrating the sensitivities of elements using raw PbTe powder as a standard. The similar ratios of two elements in wires and powders suggest no preferential evaporation or diffusion in glass matrix occurs during the fiber drawing. But, the content of oxygen increases after multiple drawing steps, probably due to the high pressure of residual oxygen in the glass tube. A rigaku X-ray diffraction (XRD) diffractometer with Cu-$K\alpha$ line radiation has been used to determine the crystallography of glass-coated wires. Figure 4B shows the XRD spectra collected from PbTe powder, wires from the first, second, and third draws (from top to bottom). The intensities of the diffraction peaks of the second-drawn samples are larger than those of the third-drawn sample. The first-drawn sample has shown lowest peak intensities, which can be induced by misalignment of X-ray beam on microwires. A sharp peak corresponding to the [200] plane of PbTe are observed at 27.15° for three samples; while intensities of peaks that correspond to the [111], [220], and [222] planes vary after each draw. The intensity changes are resorted to the structures of glass−PbTe composites. Glass sidewall may preferentially facilitate the formation of certain crystallography structures or stabilize high-energy planes such as [220] or [222]. When the wire diameters decrease, the wall effects are more significant, and thus the relative intensity of [220] or [222] plane is increased. The diffraction patterns of the second and third draw fibers show an additional peak at 24°, which is due to the partial oxidation of PbTe to PbO (32).

In FDN, the total mass of the preform is conserved during the fiber drawing, when the length of fiber increases, both the diameters of wires and interwire spacing decrease. The diameter and spacing of micro/nanowires are determined by geometries of glass tube, as well as drawing conditions. For a given preform, the size reduction, and the spacing reduction are achieved by repeating the simple draw-cut-stack process. To understand the deformation of glass tube and filling material during the size reduction process, we have measured the diameters and spacing of wires and the outer diameters of the surrounding glass. Because the glass fibers obtained after one drawing cycle offer only limited information, the short tapered pieces that are left after each drawing cycles are used to provide more information on material deformation. Basically, the tapered pieces with a continuous change of diameter from several centimeters to hundreds of micrometers are cut into thin plates of different outer diameter. Each slide is polished and etched to expose the diameter and spacing of the microwire. The diameter of each sample is measured as a function of the diameters of surrounding glass. For the first-drawn fibers, the diameter of the surrounding glass equals that of the fiber diameter. For the second-drawn fibers, the diameter of the surrounding glass is defined as the sum of the diameter and

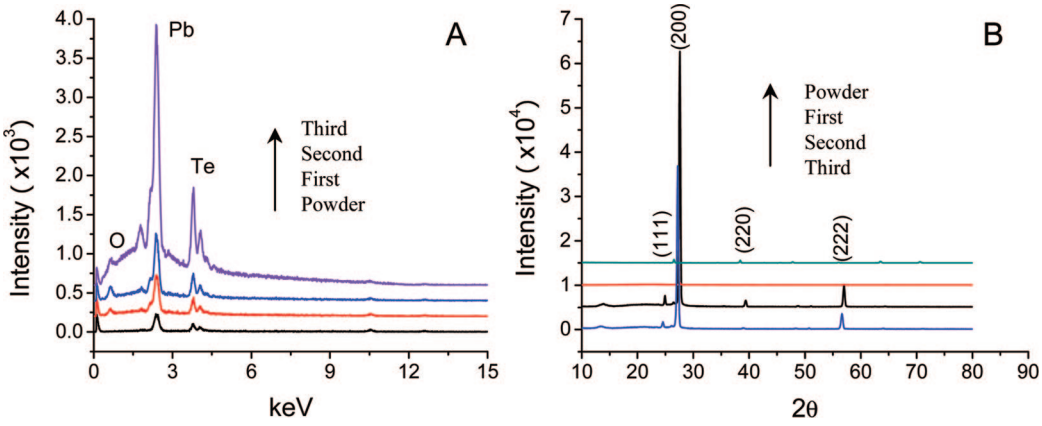

FIGURE 4. (A) EDX spectra of PbTe powder and wires obtained after the first, second, and third draws (from bottom to top); (B) XRD curves of PbTe powder and wires after the first, second, and third draws (from top to bottom).

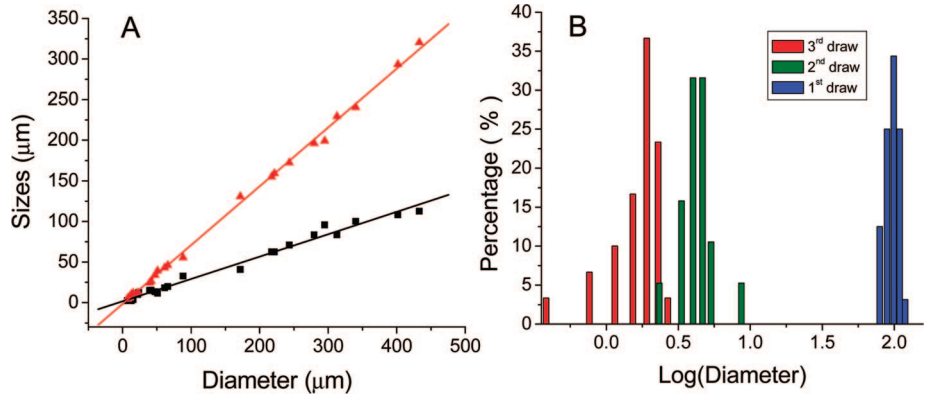

FIGURE 5. (A) Diameter (square) and spacing (triangle) reductions as functions of the diameter of surrounding glasses. (B) Size distributions for the first, second and third draw.

the spacing of the wire. Figure 5 shows that as the diameters of the surrounding glass decrease, the diameter (square) and the spacing (triangle) of the PbTe wires decrease linearly, suggesting the diameter and the spacing of wire are dependent on the diameter of the surrounding glass. In general, Figure 5A confirms as the diameter of glass shell decrease, the diameter and the spacing of the PbTe wires will decrease. The two lines will reach a point where the linear extrapolation is no longer effective, probably due to the strong interface effect. The size distributions of PbTe wires after each draw cycle are shown in Figure 5B. The average diameters for the first, second, and third draws are 90, 4, and 2 μm, respectively.

From another aspect, we have derived the relation between the diameter and spacing of the PbTe wires and the fiber-draw cycles by taking into account of the contributions from the ratio of coefficients of thermal expansion. The wire diameters after the first, second, and third draw cycles can be derived by using the following equation:

$$d_n = \frac{(\Phi_f)^n r}{[2(R+T)]^{n-1}(r+t)} \qquad (1)$$

where d_n is the diameter of wires after n draws, Φ_f is the outer diameter of fiber after n draws, r is the inner radius of the glass tube in the first draw cycle, R is the inner radius of the tube in the second and third draw cycle, t is the thickness of the glass tube in the first draw, and T is the thickness of the glass tube used to encircle the fiber bundles obtained in the second and the third draws. The interwire spacing during the fiber drawing process can be derived from the following equation

$$l_n = \frac{(\Phi_f)^n t}{[2(R+T)]^{n-1}(r+t)} \qquad (2)$$

where l_n is the spacing between two wires after n draws. Φ_f, R, T, r, and t have the same meaning as those in the eq 1. Using the dimensions of glass tube, and the outer diameter of the fiber bundles, we have calculated the diameter and spacing after the first and the second drawing cycles. Furthermore, the actual diameter and spacing after the first and the second drawing cycles are measured from the according SEM images. Both sets of data are indicated in Table 1. Because the starting material is filled in powder form, the glass tube's diameter will shrink more to enclose the melted PbTe wires. We have derived the volume of the interstitial room between powders and normalized the geometry of the starting glass tube. The actual volume of the filling material (i.e., the PbTe powder) is derived from the weight and the density of powder. The normalized inner diameter of the initial glass tube is 1.5 mm. As shown in the figure, the ratios of calculated diameter and spacing for the first, second, and third draws are close to each other (0.27, 0.25, and 0.245). Meanwhile, the ratios of measured diameter and spacing are also close to each other (0.28, 0.267, and 0.24). In case of the last draw, the interwire spacing is determined as the shortest distance between two PbTe

Table 1. Diameter and Spacing of Wires after the First, Second and Third Drawing

	D_{cal} (μm)	S_{cal} (μm)	D_{cal}/S_{cal}	D_{exp} (μm)	S_{exp} (μm)	D_{exp}/S_{exp}
1st draw	92.6	345	0.27	95.0	333	0.28
2nd draw	4.0	16.0	0.25	5.0	18.7	0.267
3nd draw[a]	0.13	0.53	0.245	0.40	1.67[b]	0.24

[a] The third draw is a combination of a normal drawing and a further extension. [b] The shortest distance in the SEM image is used as the spacing.

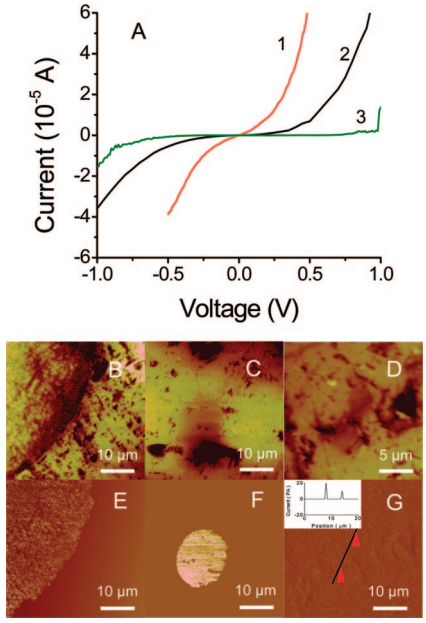

FIGURE 6. (A) $I-V$ curves measured across arrays of wires obtained from the first, second, and third draw cycles (curves 1, 2, and 3). AFM and C-AFM images of wires obtained after the (B, E) first, (C, F) second, and (D, G) third draws.

nanowires from high-resolution images, which is reasonable because some nanowires may be covered by glass debris after the polishing process.

We have measured the electrical conductivities of PbTe micro/nanowires embedded in the glass by depositing thin films of silver paste on two parallel or adjacent (but not connected) sides of the glass-PbTe cube. The current versus voltage curves ($I-V$ curves) of the PbTe wires are collected by using a Keithley 2400 sourcemeter. Figure 6A shows the $I-V$ curves of the glass-wire composites after the first, second, and third drawing cycles (indicated as 1, 2, and 3, respectively), where semiconductive behaviors of PbTe wires are evident. The measured resistance values are converted to resistivities by considering the geometry and the number density of wires. The resistances are measured using a digital multimeter as 25 kΩ, 714 kΩ, and 40 MΩ for the first, second, and third draw wires, from which the resistivities are then determined as 59 Ω m, 2.5 kΩ m, and 3.4 MΩ m, respectively. Compared to the resistance of PbTe, the contact resistance of the silver paste (0.5 Ω) can be omitted. Further, we have measured the electrical conductivity of single wires embedded inside glass using a conductive atomic force microscope (C-AFM). A glass-wire composite is polished at two parallel sides, and one side is coated with conductive silver paste. A multimode AFM with Pt–Ir thin film coated conductive tip is used to simultaneously collect the topographic and conductive images. The thicknesses of the plate, (i.e., the length of microwires) are 2 mm. Figure 6B–G shows the AFM and C-AFM images of wires obtained from the first, second, and third drawing cycle, respectively. Even if composite surfaces are polished using finest grade of grit, the topographic AFM images show that the surfaces are relatively rough, with a root-mean-square (rms) roughness of 100 nm. In contrast to the topographic images, C-AFM images are smooth and show several distinct features. (1) The glass region shows lower conductivity than PbTe regions; if the effective contact area between the C-AFM tip and the wires is 50 nm, the resistivities obtained from C-AFM images are 196 Ω m, 0.5 Ω m (1 V), and 200 MΩ m (10 V) for single wires obtained in the first, second, and third drawing, respectively. These values are close to those of bulk values. The small difference could be induced by the fact that the bulk results are dominated by highly conductive wires, which is not the case for single wire measurement. (2) The conductivity of single wire indicates heterogeneity. Considering the high aspect ratio of the C-AFM tip, it is possible certain areas on the rough, though polished, microwires are not accessible to the tip, thus showing high contact resistance. To exclude the uncertainty related to C-AFM measurements, we have embedded a normal 10 MΩ resistor in an epoxy resin, and polished both sides of the resin as that of glass-wire composite. The resistance from C-AFM measurement is close to 10 MΩ, thus confirming the validity of C-AFM measurement. (3) Other than the high resistance contact, the higher resistivities could be induced by the oxidation of PbTe during the drawing or annealing steps, or the polishing process. Another possibility is that the micro/nanowires could contain some pores during densification process, which may be responsible for the fracture of the long wires into micrometer wires. Because the bulk and single wire measurements are dealing with composite plates with thickness of several millimeters, the likelihood of encountering fractures increase, thus leading to higher resistivities. Previous research has shown that PbTe can be either an n- or p-type material by slightly unbalancing the stoichiometric $Pb_{50}Te_{50}$ ratio (33). We are working on composition-dependent gating effect of PbTe wires.

In summary, a new method to make 3D ordered micro/nanowire arrays by assembling fibrous building blocks is described. FDN is used to make fibrous building blocks (FBBs) of semiconductor materials with controlled diameters and interwire spacing. The glass matrix can be polished to expose embedded wires, or etched to exposed wires. The electrical measurements confirm the semiconductive behaviors of micro/nanowires. The combination of programmed size reduction, and the 3D assembly of FBBs enables the facile fabrication of ordered nanowires for a variety of device applications.

Acknowledgment. Y.H. and Z.M. have contributed equally to this paper. The project was supported by a New Investigator Award from the James and Esther King Biomedical Program of the Florida Department of Health, a Starter G

grant from the Petroleum Research Fund of the American Chemical Society, a research grant from National Aeronautics and Space Administration through the Florida Space Grant Consortium, a research grant from Air Force Research Laboratory of the United States, and an in-house research grant from the University of Central Florida. Most characterizations were performed at the Materials Characterization Facility.

REFERENCES AND NOTES

(1) Li, Y.; Qian, F.; Xiang, J.; Lieber, C. M. *Mater. Today* **2006**, *9*, 18.
(2) Nakayama, Y.; Pauzauskie, P. J.; Radenovic, A.; Onorato, R. M.; Saykally, R. J.; Liphardt, J.; Yang, P. *Nature* **2007**, *447*, 1098.
(3) Favier, F.; Walter, E.; Zach, M.; Benter, T.; Penner, R. M. *Science* **2001**, *293*, 2227.
(4) Law, M.; Goldberger, J.; Yang, P. *Annu. Rev. Mater. Res.* **2004**, *34*, 83.
(5) Zhan, J. H.; Yang, X. G.; Wang, D. W.; Li, S. D.; Xie, Y.; Xia, Y. N.; Qian, Y. T. *Adv. Mater.* **2000**, *12*, 1348.
(6) Che, G.; Lakshmi, B. B.; Fisher, E. R.; Martin, C. R. *Nature* **1998**, *393*, 346.
(7) Hanrath, T.; Korgel, B. A. *Adv. Mater.* **2003**, *15*, 437.
(8) Novotny, C. J.; Yu, E. T.; Yu, P. K. L. *Nano Lett.* **2008**, *8*, 775.
(9) Lee, S. H.; Minegishi, T.; Park, J. S.; Park, S. H.; Ha, J.-S.; Lee, H.-J.; Ahn, S.; Kim, J.; Jeon, H.; Yao, T. *Nano Lett.* **2008**, *8*, 2419.
(10) Gudiksen, M. S.; Wang, J.; Lieber, C. M. *J. Phys. Chem. B* **2001**, *105*, 4062.
(11) Zhao, S.; Roberge, H.; Yelon, A.; Verest, T. *J. Am. Chem. Soc.* **2006**, *38*, 12352.
(12) He, J.-H.; Wan, Y.-Q.; Yu, J.-Y. *Polymer* **2005**, *46*, 2799.
(13) Donald, I. W. *J. Mater. Sci.* **1987**, *22*, 2661.
(14) Tong, T.; Mazur, E. *J. Non-Cryst. Solids* **2008**, *354*, 1240.
(15) Huang, Y.; Duan, X.; Wei, Q.; Lieber, C. M. *Science* **2001**, *291*, 630.
(16) Ryan, K. M.; Mastroianni, A.; Stancil, K. A.; Liu, H.; Alivisatos, A. P. *Nano Lett.* **2006**, *6*, 1479.
(17) Yu, G.; Cao, A.; Lieber, C. M. *Nat. Nanotechnol.* **2007**, *2*, 372.
(18) Pauzauskie, P. J.; Radenovic, A.; Trepagnier, E.; Shoroff, H.; Yang, P.; Liphardt, J. *Nat. Mater.* **2006**, *5*, 97.
(19) Yang, Y.; Kung, S. C.; Taggart, D. K.; Xiang, C.; Yang, F.; Brown, M. A.; Guell, A. G.; Kruse, T. J.; Hemminger, J. C.; Penner, R. M. *Nano Lett.* **2008**, *8*, 2447.
(20) Su, M.; Li, Y.; Maynor, B.; Buldum, A.; Lu, J. P.; Liu, J. *J. Phys. Chem. B* **2000**, *104*, 6305.
(21) Zhou, J.; Liu, J.; Wang, X.; Song, J.; Tummala, R.; Xu, N. S.; Wang, Z. L. *Small* **2007**, *3*, 622.
(22) Gao, P. X.; Lao, C. S.; Hughes, W. L.; Wang, Z. L. *Chem. Phys. Lett.* **2005**, *408*, 174.
(23) Zhou, J.; Ding, Y.; Deng, S. Z.; Gong, L.; Xu, N. S.; Wang, Z. L. *Adv. Mater.* **2005**, *17*, 2107.
(24) Ponzoni, A.; Comini, E.; Sberveglieri, G.; Zhou, J.; Deng, S. Z.; Xu, N. S.; Ding, Y.; Wang, Z. L. *Appl. Phys. Lett.* **2006**, *88*, 203101.
(25) Wang, D.; Luo, H.; Kou, R.; Gil, M. P.; Xiao, S.; Golub, V. O.; Yang, Z.; Brinker, C. J.; Lu, Y. *Angew. Chem., Int. Ed.* **2004**, 116.
(26) Zhu, J.; Peng, H.; Chan, C.; Jarausch, K.; Zhang, X.; Cui, Y. *Nano Lett.* **2007**, *7*, 1095.
(27) Bierman, M. J.; Lau, Y. K. A.; Jin, S. *Nano Lett.* **2007**, *7*, 2907.
(28) Levi, F. P. *Nature* **1959**, *183*, 1251.
(29) Tonucci, R. J.; Justus, B. L.; Campillo, A. J.; Ford, C. E. *Science* **1992**, *258*, 783.
(30) D'Urso, B. R.; Simpson, J. T.; Kalyanaraman, M. *Appl. Phys. Lett.* **2007**, *90*, 044102.
(31) Zhang, X.; Ma, Z.; Yuan, Z.-Y.; Su, M. *Adv. Mater.* **2008**, *20*, 1310.
(32) Jia, B.; Gao, L. *Mater. Chem. Phys.* **2006**, *100*, 352.
(33) Perrin, B.; Hedgcock, F. T. *J. Phys. C: Solid State Phys.* **1982**, *15*, 6037.

AM800171T